Published in final edited form as:
Earth Planet Sci Lett. 2017 June 1; 467: 157–166. doi:10.1016/j.epsl.2017.02.044.

Characterizing cosmochemical materials with genetic affinities to the Earth: Genetic and chronological diversity within the IAB iron meteorite complex

Emily A. Worsham[a,b,*], **Katherine R. Bermingham**[a], and **Richard J. Walker**[a]

[a]Department of Geology, University of Maryland, College Park, MD 20742, USA

[b]Institut für Planetologie, University of Münster, Münster 48149, Germany

Abstract

The IAB iron meteorite complex consists of a main group (MG) and five chemical subgroups (sLL, sLM, sLH, sHL, and sHH). Here, mass-independent Mo and radiogenic 182W isotope compositions are reported for IAB complex meteorites to evaluate the genetics and chronology, respectively, of the MG and subgroups. Osmium isotopes are used to correct for cosmic ray exposure effects on isotopes of Mo andW. The MG and three subgroups (i.e., sLL, sLM, and sLH), characterized by low Au abundances, have the same Mo isotopic compositions within analytical uncertainty, consistent with a common genetic origin. These meteorites, together with winonaites, are the only cosmochemical materials yet identified with Mo isotopic compositions that are identical to Earth. The Mo isotopic compositions of two subgroups characterized by higher Au abundances (sHL and sHH) are identical to one another within uncertainty, but differ from the low Au subgroups, indicating derivation from genetically distinct materials.

The MG has a 182W, post calcium–aluminum inclusion (CAI) formation model age of 3.4 ±0.7Ma. One of the low Au subgroups (sLM) is ~1.7 Ma younger, whereas the high Au subgroups are ~1.5–3 Ma older. The new Mo–W data, coupled with chemical data, indicate that the MG and the low Au subgroups formed in different impact-generated melts, some of which evidently formed on a chemically disparate, but genetically identical parent body. The high Au subgroups likely formed via core-formation processes on separate, internally-heated parent bodies from other IAB subgroups. The IAB complex meteorites fall on a linear trend defined by $^{94}Mo/^{96}Mo$ vs. $^{95}Mo/^{96}Mo$, along with most other iron meteorite groups. Variation along this line was caused by mixing between at least two nebular components. One component was likely a pure *s*-process enriched nucleosynthetic carrier, and the other a homogenized nebular component. Sombrerete, currently classified as an sHL iron, has a Mo isotopic composition that is distinct from all IAB complex meteorites analyzed here. Along with group IVB iron meteorites and some ungrouped iron meteorites, it falls on a separate line from other meteorites which may reflect addition of an *r*-process-enriched component, and it should no longer be classified as a IAB iron.

*Corresponding author at: Institut für Planetologie, University of Münster, Münster, 48149 Germany. eworsha1@umd.edu, worsham@uni-muenster.de (E.A. Worsham).

Appendix A. Supplementary material
Supplementary material related to this article can be found online at http://dx.doi.org/10.1016/j.epsl.2017.02.044.

Keywords

IAB iron meteorite; osmium isotope; molybdenum isotope; tungsten isotope; genetics; chronology

1. Introduction

"Magmatic" iron meteorite groups, including IIAB, IIIAB, IVA, and IVB, likely originated in the cores of distinct, differentiated planetesimals, and sample portions of the fractional crystallization sequence by which they crystallized (e.g., Lovering, 1957; Scott, 1972). "Non-magmatic" groups, including the IAB complex and the IIE group, have chemical compositions that cannot be produced by simple fractional crystallization (Scott, 1972). "Un-grouped" iron meteorites have chemical compositions that do not fit into any recognized groups.

The IAB complex iron meteorites are chemically and texturally distinct from the magmatic iron groups. The complex includes a main group and five subgroups, which were originally defined by their Au and Ni abundances, and, thus, have corresponding nomenclature (Wasson and Kallemeyn, 2002). In this nomenclature, the "s" stands for "subgroup", the first capital letter stands for Low or High Au, and the last letter stands for Low, Medium, or High Ni. The previously defined IIICD iron meteorite group corresponds to the sLM and sLH subgroups. Previous studies have shown that the subgroups cannot be related to one another by crystal–liquid fractionation processes, and therefore, likely originated in separate parental melts (e.g., Wasson and Kallemeyn, 2002; Worsham et al., 2016a). Winonaites are primitive achondrites that have chemical and O isotopic compositions similar to silicate inclusions in some IAB meteorites. This has led to the suggestion that they are from the same parent body as IAB meteorites (e.g., Bild, 1977; Clayton and Mayeda, 1996).

The proposed mechanisms by which the IAB complex, and possibly winonaites, formed are varied with respect to internal (e.g., ^{26}Al) or external (e.g., impact) heating on either a partially differentiated or undifferentiated parent body (e.g., Benedix et al., 2000; Wasson and Kallemeyn, 2002). One way to investigate the origin of the IAB complex is to employ isotopic genetic tracing and chronological tools to examine the MG and subgroups of the complex. Parent body-specific isotope anomalies have been observed at the bulk meteorite scale for a variety of elements, including O (Clayton and Mayeda, 1996), Ti (Trinquier et al., 2009), Ru (Fischer-Gödde et al., 2015), and Mo (Dauphas et al., 2002a; Burkhardt et al., 2011). With the exception of O, isotopic variability in these elements between meteorite groups has been attributed to nucleosynthetic effects, which likely originated as a result of inhomogeneous mixing and/or thermal processing of isotopically diverse presolar materials.

Molybdenum consists of seven stable isotopes which are synthesized by three nucleosynthetic processes; the *p*-process (^{92}Mo and ^{94}Mo), the *s*-process (trace ^{94}Mo, ^{95}Mo, ^{96}Mo, ^{97}Mo ^{98}Mo), and the *r*-process (^{95}Mo, ^{97}Mo, ^{98}Mo, ^{100}Mo; Burbidge et al., 1957). The variety of nucleosynthetic processes represented in Mo isotopes, and its isotopic variability among planetary bodies, makes Mo an ideal genetic tracer of the relative proportions of diverse presolar carriers in solar system materials (e.g., Dauphas et al., 2002a; Yin et al., 2002; Burkhardt et al., 2011). By measuring the Mo isotopic composition of IAB

meteorites from the MG and each subgroup, it can be assessed whether any originated on separate parent bodies.

Determining the relative timing of metal-silicate segregation of the various IAB subgroups may also help to clarify their chronological interrelations. The timing of core formation on magmatic iron meteorite parent bodies has commonly been assessed using the short-lived ^{182}Hf–^{182}W chronometer (e.g., Lee and Halliday, 1996; Kruijer et al., 2014a). Hafnium-182, which is lithophile, decays to ^{182}W, which is siderophile, through double β^- decay with a half-life of 8.9 Myr (Vockenhuber et al., 2004). Hafnium and W are, thus, strongly fractionated during metal-silicate segregation, with metals recording the ^{182}W composition at the time that metal-silicate equilibration ends. Model ages of metal-silicate segregation can be calculated relative to the solar system initial ^{182}W/^{184}W, recorded in Ca–Al rich inclusions (CAI; Kruijer et al., 2014b), which are the earliest condensates from the solar nebula.

Model ages of metal-silicate segregation can give insight into whether the dominant heat source which facilitated metallic melting was internal or external. Radioactive decay of short-lived nuclides, such as ^{26}Al, was likely the dominant internal heat source by which planetesimals differentiated in the early solar system (e.g., Lee et al., 1977). As the half-life of ^{26}Al is ~0.7 Ma, it was largely extinct by ~4 Ma after CAI formation (Norris et al., 1983). Most magmatic iron meteorite parent bodies differentiated within the first 2–3 Ma of solar system evolution, consistent with ^{26}Al heating (e.g., Kruijer et al., 2014a). By contrast, Schulz et al. (2012) reported model ages >5 Ma for IAB irons, suggesting that impact heating may have been the source of metal segregation. A detailed assessment of the ^{182}W in the IAB MG and subgroups would, therefore, provide further opportunity to distinguish between ^{26}Alor impact-generated IAB complex irons.

The isotopic compositions of meteorites are subject to modification by cosmic ray exposure (CRE). Both the Mo and W isotopic compositions of some iron meteorites may require corrections, depending on the duration of exposure, the neutron fluence conditions, and the shielding depth of the sample (e.g., Masarik, 1997; Markowski et al., 2006; Qin et al., 2015). Certain Os isotopes are typically homogeneous at the bulk meteorite scale, but are affected in predictable ways by CRE, so they are used here as a neutron fluence dosimeter to monitor and correct for CRE effects (e.g., Walker, 2012; Wittig et al., 2013).

2. Samples

Most samples examined in this study were obtained from the Division of Meteorites, Department of Mineral Sciences, Smithsonian Institution, National Museum of Natural History (see Table S1). Northwest Africa 725 (NWA 725) was obtained from the Lunar and Planetary Institute. For IAB complex iron meteorites, Mo, W, and Os isotope data were obtained from adjacent pieces to those used for highly siderophile element (HSE) and ^{187}Re–^{187}Os analyses (Worsham et al., 2016a). Here, a variety of primitive achondrites, including two winonaites (Winona and HAH 193), a lodranite (a metal slice from GRA 95209), and NWA 725 are considered as possible genetic relations to the IAB complex irons. Although NWA 725 is currently classified by the *Meteoritical Society* as an acapulcoite, its

O isotopic composition is similar to winonaite NWA 1463, and silicates from IAB iron meteorites (Greenwood et al., 2012). Therefore, this sample is compared both to the winonaites and the lodranite, because lodranites and acapulcoites likely originated on the same parent body (e.g., Clayton and Mayeda, 1996). Magmatic iron meteorites from groups IVB, IVA, IIIAB, and IC, ungrouped iron meteorites, ordinary chondrites, and an enstatite chondrite were also analyzed for their Mo isotopic compositions to make comparisons with the IAB complex meteorites.

3. Analytical methods

3.1. Chemical separation and purification procedures

Molybdenum, W, and Os isotopic compositions were obtained using methods previously described (Cook et al., 2004; Touboul and Walker, 2012; Walker, 2012; Worsham et al., 2016b; Archer et al., 2017; see SM for details). Iron meteorites were cut into 0.5–2.5 g pieces for Mo and W analyses. Adjacent 0.1–0.3 g pieces were cut for Os analyses for most meteorites, except where an aliquot was taken from the digestion used for Mo or W analysis. Molybdenum from some of the IAB irons was obtained as a byproduct of the W chemistry (Table S1).

Osmium was separated and purified using solvent extraction and microdistillation (Cohen and Waters, 1996; Birck et al., 1997). The Os total analytical blank was negligible for all samples, comprising <0.1% of the total Os extracted, averaging 4 ±2 pg (2SD; $n = 7$). Molybdenum separation and purification was achieved using a 2-stage anion exchange chromatographic procedure (Worsham et al., 2016b). The total analytical blank ranged from 1–5 ng (2SD; $n = 3$) and comprised <1% of the Mo extracted, which was negligible for all analyses. Tungsten was separated and purified from the sample matrix using a 4-stage cation and anion chromatographic procedure (Touboul and Walker, 2012). The total analytical blank for these procedures was 1 ng ($n = 1$), which constituted <0.5% of the total W extracted.

3.2. Mass spectrometry

Osmium and W analyses were conducted using a *Thermo-Fisher Triton* thermal ionization mass spectrometer (operated in negative ionization mode; N-TIMS), and Mo analyses were conducted using a *Thermo-Fisher Triton Plus* N-TIMS, both at the University of Maryland (see SM for details).

Osmium isotope data were normalized to $^{192}Os/^{188}Os = 3.08271$ (Allègre and Luck, 1980) to correct for instrumental and natural mass-fractionation. The long term external reproducibilities of $^{189}Os/^{188}Os$ and $^{190}Os/^{188}Os$ were ±5.6 ppm and ± 7.2 ppm (2SD), respectively, determined by repeated analyses of an Os reference material ($n = 28$).

Molybdenum was measured along with an *in situ* measurement of $^{18}O/^{16}O$ which was used for correction of trioxide iso-bars. Data were normalized to $^{98}Mo/^{96}Mo = 1.453171$ (Lu and Masuda, 1994). The long-term external reproducibility (2SD) over 13 months was ±107 ppm for ^{92}Mo, 37 ppm for ^{94}Mo, 23 ppm for ^{95}Mo, 5.4 ppm for ^{97}Mo, and 32 ppm for ^{100}Mo ($n = 48$).

Analytical procedures for analysis of W were adapted from Touboul and Walker (2012) and Archer et al. (2017). The analytical procedures evolved during the course of this study. Approximately half of the samples were measured using the technique of Touboul and Walker (2012) (termed "method I"). These data were corrected using a second-order oxide correction to mitigate the effect of variable oxygen isotope compositions on the precision of the W analyses (Touboul and Walker, 2012). Recent developments allowed for an *in situ* oxide correction, as with Mo analyses (Archer et al., 2017). Thus, the other half of the samples were measured and corrected using the measured $^{18}O/^{16}O$ (method II). Tungsten data were fractionation-corrected using $^{186}W/^{183}W = 1.98590$ and $^{186}W/^{184}W = 0.92767$ (Volkening et al., 1991). In both cases, the $^{182}W/^{184}W$ ratio is reported. The external reproducibilities (2SD) of $^{182}W/^{184}W$ were ±4.5 ppm ($n = 30$) for method I and ±4.4 ppm ($n = 31$) for method II, when the data were fractionation-corrected using $^{186}W/^{183}W$. The $^{183}W/^{184}W$ ratio was also measured using method II (see SM).

4. Results

4.1. Cosmic ray exposure corrections

Cosmic ray exposure can modify the original isotopic composition of most elements. The CRE effects are dependent, in part, on the depth within a sample, thus it is important to monitor and correct for CRE effects using the same meteorite piece or a piece from within a few cm of samples analyzed for other isotopic compositions (Markowski et al., 2006). Osmium isotopes do not show resolvable nucleosynthetic effects on the bulk meteorite scale, so the Os isotopic compositions of bulk meteorites reflect CRE effects, as well as the ingrowth of radiogenic ^{186}Os and ^{187}Os (Walker, 2012). Consequently, Os can serve as a siderophile element CRE dosimeter (Wittig et al., 2013). Values for $\mu^{189}Os$, where μ notation is the deviation of the measured ratio from that of terrestrial standards, multiplied by 10^6, are the most useful of the Os isotopes for use as a neutron fluence dosimeter (see SM for details).

Osmium data are reported in Table 1. New data for several magmatic irons, also analyzed by Walker (2012), are in good agreement with that study (Table S2). Osmium isotopic compositions for most of the IAB complex are within uncertainty of terrestrial values, but some samples show negative deviations in $\mu^{189}Os$, indicative of CRE effects.

Molybdenum and W isotope data that are uncorrected for CRE are reported in Tables S3–S4. Cosmic ray exposure effects have not been previously recognized in the Mo isotopic compositions of iron meteorites. Variations in the $\mu^{i}Mo$ values among meteorites from the sLL and sLM subgroups, however, are correlated with $\mu^{189}Os$, indicating that some Mo isotopes can be modified by CRE (primarily ^{95}Mo and ^{96}Mo) (Table S5, discussed in SM). The slopes of these correlations are similar to the slope observed for group IVB magmatic iron meteorites, which exhibit known CRE effects (Fig. 1a, Table S5). Well defined linear trends of $\mu^{189}Os$ vs. $\mu^{182}W$ are also observed for the MG and the sLL and sLM subgroups, which have slopes in good agreement with previous studies (Qin et al., 2015; Fig. 1b; Table S6).

The correlations between μ^{189}Os vs. μ^{i}Mo or μ^{182}W for related meteorites can be used to correct to pre-exposure isotopic compositions (Fig. 1a–b). Details regarding the two CRE correction methods used in this study for each meteorite/meteorite group can be found in the supplementary materials (Table S1). Briefly, the pre-exposure isotopic composition can be obtained by projecting the correlation of μ^{189}Os vs. μ^{i}Mo or μ^{189}Os vs. μ^{182}W to the intercept (e.g., Wittig et al., 2013), giving one pre-exposure μ^{i}Mo or μ^{182}W for a group of meteorites having a single Mo isotopic composition or metal-silicate segregation age (termed the “intercept-derived, group pre-exposure”).

The Mo or W isotopic composition of an individual meteorite can also be corrected by projecting the μ^{i}Mo or μ^{182}W value of a sample to a μ^{189}Os of zero, using the simple linear equation and well-defined slopes of correlations between μ^{189}Os vs. μ^{i}Mo or μ^{182}W. This method is here termed the “slope-derived, individual pre-exposure” method, and is necessary to correct individual meteorites from each subgroup, especially in subgroups with few members. This correction method is similar to that of Qin et al. (2015) (see SM).

4.2. CRE-corrected Mo and W isotope results

Molybdenum and W data corrected for CRE for IAB complex meteorites are provided in Tables 2–3. New Mo data for magmatic and ungrouped iron meteorites, primitive achondrites, and enstatite and ordinary chondrites are also provided in Table 2. Uncertainties for intercept-derived, group pre-exposure values are the uncertainties of the intercepts of the regressions calculated using ISOPLOT (95% confidence, Ludwig, 2003). Uncertainties for the slope-derived, individual pre-exposure values are propagated through the linear calculation of the CRE correction, combining the 2SD (number of analyses – $n \leq 3$) or 2SE ($n > 3$) uncertainties of the measurements and the uncertainties of the slopes, calculated using ISOPLOT.

The ^{97}Mo/^{96}Mo ratio is measured to the highest precision in this study and is minimally affected by CRE, as evidenced by the small effect observed in the μ^{97}Mo value of Deport (−7.5±7; 2SD), which exhibits the largest known effect in μ^{189}Os− (Fig.±1a). Thus, it is assumed that the μ^{97}Mo values of the few samples for which Os data were not collected were minimally affected. For these reasons, μ^{97}Mo is used for genetic comparisons here.

The CRE-corrected Mo isotope data for IAB complex irons, magmatic irons, and chondrites (Table 2) are in general agreement with data reported by Dauphas et al. (2002a) and Burkhardt et al. (2011) for irons and chondrites from the same groups, but the μ^{97}Mo values reported here are typically ≥2 times more precise. Most IAB complex iron meteorites have Mo isotopic compositions that are within uncertainty of the terrestrial Mo isotopic composition, represented by the average Mo isotopic composition of an *Alfa Aesar* standard (Figs. 2 and S2). The MG (μ^{97}Mo=−0.6±1.4; 2SE), sLL (μ^{97}Mo = 1.3±2.1; 2SD), sLM (μ^{97}Mo 1.= −9 3.4;±2SD), and sLH (μ^{97}Mo = −1.7 ±4 0;2SD) samples have Mo isotopic compositions that are indistinguishable from one another. By contrast, the μ^{97}Mo values for the sHL (μ^{97}Mo= 23±9; 2SD) and sHH (μ^{97}Mo = 24 ± 3; 2SD) subgroups are well resolved from the MG and other IAB subgroups. They do, however, overlap with one another, and some magmatic iron groups (e.g., IC, IVA, IIIAB). Sombrerete, which has been classified as an sHL iron (Wasson and Kallemeyn, 2002), has a μ^{97}Mo value of 57 ±5 that is much higher

than other IAB complex meteorites reported here. It overlaps with the μ^{97}Mo value of the magmatic IVB group and the ungrouped iron meteorites Chinga, Tishomingo, and Dronino.

The winonaites, Winona and HAH 193, have μ97Mo values of −1.3 ± 3.3 and 4.9 ± 3.3 that are indistinguishable, within uncertainty, of one another, and are, on average, indistinguishable from the MG and the low Au subgroups. By contrast, the acapulcoite NWA 725 and lodranite GRA 95209 have μ^{97}Mo values of 30 ± 5 and 21 ± 3, respectively, both of which are higher than the MG and winonaites. These samples are currently resolved from one another, but both overlap with the sHL and sHH subgroup irons. Ordinary chondrites, Richardton (H5) and Allegan (H5), have μ^{97}Mo values of 30 ± 5 and 19 ± 5, respectively, that are resolved from one another. The enstatite chondrite, Saint-Sauveur (EH5), has Mo isotopic composition (μ^{97}Mo = 11 ± 5) that is higher than the terrestrial Mo isotopic composition.

The CRE-corrected μ^{182}W values are shown in Fig. 3. Tungsten isotope data were not collected for sLH irons or Mount Magnet (sHH), due to their low W concentrations. For the MG, the intercept-derived, group pre-exposure μ^{182}W value is −312 ± 6. This is resolved from the group pre-exposure μ^{182}W values for the sLL (μ^{182}W =−297 ±8) and sLM (μ^{182}W =−297 ±5) subgroups. The sHL and sHH samples have resolvably lower slope-derived, individual pre-exposure μ^{182}W of −316 10 that is higher than sHL and sHH, yet is within uncertainty of± the MG. The two samples from the sHH subgroup analyzed, ALHA 80104 and Kofa, have different μ^{182}W values of −345 ± 5 and −330 ± 5, respectively. Although the magnitude of CRE modification on the value for Kofa is unknown (see SM), the difference between these meteorites is not a result of unaccounted for CRE effects. Correction for CRE could only increase its μ^{182}W value. The μ^{182}W value for the MG is within uncertainty of the IVB and IID magmatic iron groups, whereas the μ^{182}W values of sHL and sHH samples overlap with those of the IVA, IIAB, and IIIAB magmatic iron groups (Kruijer et al., 2014a) (Fig. 3).

The pre-exposure W isotopic compositions for the MG and sLL subgroup are lower (by 14 to 29 ppm) than the combined IAB, pre-exposure μ^{182}W value reported by Schulz et al. (2012) of − 283 ± 3. The reason for the offset is unclear. Schulz et al. (2012) used the regression of CRE ages from the literature vs. μ^{182}W to obtain the pre-exposure μ^{182}W, combining data for both MG and sLL iron meteorites. Cosmic ray exposure ages, however, are not directly related to neutron fluence, because CRE ages are determined using cosmogenic noble gasses which are produced by higher energy protons and neutrons than the thermal neutrons that modify W isotopic compositions. Further, the application of CRE ages obtained from different meteorite pieces from those analyzed for μ^{182}W likely does not account for the depth-dependence of CRE effects (e.g., Masarik, 1997; Markowski et al., 2006; Qin et al., 2015). Although Sm isotopes were measured by Schulz et al. (2012) to monitor for neutron fluence and different shielding conditions, these were not used for correction of the CRE ages or the W isotopic compositions.

5. Discussion

5.1. IAB subgroup genetics inferred by Mo isotopes

The indistinguishable Mo isotope ratios for the MG and the sLL, sLM, and sLH subgroups are consistent with their generation on either the same parent body, or multiple genetically related parent bodies (Fig. 2). Formation of MG and sLL meteorites on a single parent body is supported by the compositional and mineralogical similarity of MG and sLL metals and silicates (Wasson and Kallemeyn, 2002; Benedix et al., 2000). Despite the similarities, the MG and sLL subgroup likely crystallized from separate parental melts. This is indicated by the differences in Ni, Au, and Pd abundances between the MG and sLL subgroup, which cannot be accounted for by crystal–liquid fractionation from a common melt, but could result from different degrees of partial melting of an identical source (Wasson and Kallemeyn, 2002; Worsham et al., 2016a). Thus, if the parental melts of these groups were generated as a result of impact (e.g., Wasson and Kallemeyn, 2002), more than one impact was required to produce these compositions. Likewise, if these subgroups melted due to internal heating and partial differentiation of the parent body (e.g., Benedix et al., 2000), they must have crystallized in different metal diapirs or melt pockets.

Relative to the MG and sLL subgroup, the sLM and sLH subgroups have essentially identical μ^{97}Mo values, yet are characterized by different major and trace element abundances. The major and trace element abundances of the sLM and sLH subgroups are quite similar to one another (e.g., Wasson and Kallemeyn, 2002). Despite μ^{97}Mo values that overlap with the MG and sLL subgroup, the absolute and relative abundances of the HSE suggest the sLM and sLH subgroups formed on a separate parent body from the MG and sLL subgroup (Worsham et al., 2016a). Therefore, at least two parent bodies are represented in the IAB complex meteorites which have μ^{97}Mo values of approximately zero.

The sHL and sHH subgroups are chemically distinct from the other IAB complex meteorites due to their higher abundances of Au. They are distinct from one another due to the low and high Ni abundances in the sHL and sHH subgroups, respectively (Wasson and Kallemeyn, 2002). These subgroups are characterized by a wide range in siderophile element compositions and relatively few members. Consequently, prior studies noted the difficulty of assigning these meteorites to genetically significant groups (e.g., Wasson and Kallemeyn, 2002). The Mo isotopic compositions of these two subgroups are distinct from the MG and low Au IAB subgroups, but indistinguishable from one another (with the exception of Sombrerete). This indicates that the sHL and sHH subgroups formed on at least one additional parent body from any of the low Au subgroups.

Sombrerete was tentatively assigned to the sHL subgroup by Wasson and Kallemeyn (2002), based on its siderophile element abundances, yet it has a distinct μ^{97}Mo compared to all other IAB iron meteorites studied here. It is also characterized by a distinct Δ^{17}O, unusually high P abundance, and non-chondritic silicate inclusions, compared with other IAB complex meteorites (Clayton and Mayeda, 1996; Ruzicka et al., 2006). The Mo isotope data support the conclusion of Ruzicka et al. (2006), that Sombrerete is an ungrouped iron that is not related to the IAB complex. Henceforth, Chebankol and Quarat al Hanish are considered the only sHL meteorites studied here.

The identical Mo isotopic compositions of the low-Au subgroups and the two winonaites studied here support the proposed genetic link between the winonaites and the IAB MG and some subgroups. Thus, winonaites likely formed on the same parent body as either the MG and sLL subgroup, or the sLM and sLH subgroups. Mineralogical and major and trace element abundance similarities between winonaites and MG and sLL silicates indicate that the former is more likely (e.g., Benedix et al., 2000). Moreover, because of these mineralogical similarities, the Mo isotope data suggest that the silicates and metals in the low Au IAB meteorites were co-genetic.

The Mo isotopic composition of NWA 725, classified as an acapulcoite, is well resolved from that of the IAB MG, but overlaps with the high Au subgroups. Thus, despite similarities in $\Delta^{17}O$, the Mo isotopic composition indicates that NWA 725 is not related to winonaites or the IAB MG. Further, the $\mu^{97}Mo$ value of NWA 725 is higher than lodranite GRA 95209, although they both overlap with the high Au subgroups. This, in addition to the O isotopic composition of NWA 725 (Greenwood et al., 2012), suggests that it is not an acapulcoite and should instead be classified as an un-grouped primitive achondrite. The data permit a genetic relation of either NWA 725 or GRA 95209 to the high Au subgroups. No $\Delta^{17}O$ data for silicates in the sHL and sHH irons currently exist, so a genetic link between these meteorites and the high Au subgroups cannot be further evaluated at this time.

5.2. IAB subgroup metal–silicate segregation chronology

Metal–silicate Hf–W segregation model ages (t_{CAI}) are calculated relative to a CAI initial $\mu^{182}W = -349 \pm 7$ (Kruijer et al., 2014b), assuming precursors with a chondritic $^{180}Hf/^{184}W=1.29 \pm 0.09$, which corresponds to a present-day chondritic $\mu^{182}W = -190 \pm 10$ (Kleine et al., 2004). While these 2-stage model ages most likely represent primary relative metal-silicate segregation ages, it should be noted that differences in model age could also reflect different Hf/W ratios in the precursor materials, or more complex differentiation and/or mixing scenarios than are presented below (see SM for more discussion).

The intercept-derived MG $\mu^{182}W$ of −312 ±6 corresponds to a model age of 3.4 ±0.7Ma after CAI formation (Fig. 3). Model ages for the sLL and sLM subgroups are 5.0±1.0 the ± and 5.1±0.6 Ma, respectively. Despite the resolved $\mu^{182}W$ values of the MG and the sLL subgroup, the model ages are indistinguishable, given the other uncertainties associated with the model age calculation (see SM section 6.2). However, the ~5 Ma segregation ages of the sLL and sLM subgroups are younger than those of magmatic iron meteorite groups (e.g., Kruijer et al., 2014a) and are beyond the effective lifetime of ^{26}Al. This suggests that impact-generated heating was the cause of melting in these subgroups, if they formed on small parent bodies or near-surface on larger parent bodies.

The model age of the MG of 3.4±0.7 Ma is nearing the end of the effective lifetime of ^{26}Al, but it overlaps with the IVB and IID magmatic iron groups, which have model ages of 2.9 ± 0.5 and 3.1 ± 0.8, respectively (Kruijer et al., 2014a). The relative timing of core formation in the parent bodies of the magmatic irons was partly controlled by S abundance, where core formation occurred in two stages due to the lower melting temperature of FeS, relative to Fe. Therefore, bodies with higher S abundances have older segregation ages than low-S parent bodies (Kruijer et al., 2014a). As the MG likely had comparatively high initial S

abundances, similar to the IIIAB group, characterized by a metal segregation age of 1.2±0.3 Ma (Kruijer et al., 2014a; Worsham et al., 2016a), an apparent earlier metal segregation age would be expected if two-stage core formation, due to internal heating, took place. Alternately, if the MG-sLL parent body accreted relatively late, the S abundance and the segregation age may be reconciled by invoking internal heating. Although the model age of the MG suggests that its melt could have segregated due to internal heat-induced partial differentiation, the similarity of the characteristics of the MG and sLL subgroup suggests that they formed in a similar manner, as discussed in section 5.3.

In contrast to the MG and the sLL and sLM subgroups, the sHL and sHH subgroups have metal segregation ages that are well within the lifetime of ^{26}Al. The model age of each meteorite is also resolved from the MG. These metal segregation ages overlap with the magmatic iron meteorite groups, and allow that the parental melts of the sHL and sHH irons originated via internal heating and differentiation. In the case of ALHA 80104 and Kofa, the disparate ages suggest they formed in separate metal segregation events.

5.3. IAB complex formation informed by combined Mo–W isotope data

When the Mo and W isotope data are collectively considered, it is apparent that the IAB complex represents multiple parent bodies and metal-silicate segregation events. The preferred formation scenarios for each of the subgroups are shown in Fig. 4. A summary of the evidence used to reject genetic links between subgroups and estimate the number of parent bodies represented in the IAB complex is given in Table S8.

The MG and sLL subgroup probably formed on the same parent body, in two metal segregation events separated by 0 to 3 Ma. While the MG metal segregation event may have occurred during the effective lifetime of ^{26}Al, especially on a large parent body that efficiently retained internal heat, the sLL melt likely segregated too late for the decay of ^{26}Al to have been the heat source. The sLL subgroup has chondritic relative abundances of the HSE, which indicates crystallization with little chemical processing (Worsham et al., 2016a). This, in addition to the relatively late segregation age, implies that the sLL subgroup formed due to impact-generated melting.

The formation model proposed by Benedix et al. (2000) invoked partial differentiation due to internal heating of a parent body, followed by catastrophic breakup and reassembly which mixed different silicate lithologies. In this scenario, the conditions of the MG and sLL W isotopic compositions could potentially be met if partial differentiation, driven by the decay of ^{26}Al, formed the initial MG melt, and an impact into still metal-rich megaregolith produced the sLL melt. This model is not favored here, however, because the proposed breakup and reassembly event would likely have led to re-melting and/or mixing of the metal, in addition to mixing the silicate lithologies. This would likely have led to the equilibration of the W isotopic compositions of the metals and silicate, resetting the μ^{182}W values and/or erasing the small difference in μ^{182}W between the MG and sLL subgroup.

Our preferred model for the formation of the MG and sLL subgroup is the impact-generated melt model described by Wasson and Kallemeyn (2002). In this scenario, the MG melt formed via an impact into a warm, but not differentiated body. A separate impact event

formed the sLL subgroup in a different location on the same parent body. The chemical differences between the MG and sLL subgroup may be the result of different degrees of partial melting, controlled by the size of the impacts which generated the melts (e.g., Wasson and Kallemeyn, 2002). The HSE abundances in the MG indicate the occurrence of crystal–liquid fractionation and mixing effects in the melt, in contrast to the minor chemical processing estimated for the sLL melt (Worsham et al., 2016a). This suggests that the sLL event was smaller and involved less melt than the MG event.

The sLM subgroup likely formed on a separate parent body from the MG-sLL parent body (e.g., Worsham et al., 2016a) in an impact event which occurred ~1.7 Ma later than the impact which created the MG. The chemical and isotopic similarity of the sLM and sLH subgroups suggest that they formed on the same parent body (Wasson and Kallemeyn, 2002; Worsham et al., 2016a). The distinct Ni and Pd contents of these subgroups may reflect different degrees of partial melt from impacts of different sizes, or impacts into more or less metal-rich portions of the parent body.

The Mo isotopic compositions of the sHL and sHH subgroups indicate that they formed from a different nebular reservoir than the MG or other IAB complex subgroups. The metal segregation event or events were earlier than the MG, and early enough that the decay of ^{26}Al was likely the heat source which generated the melt/melts. This suggests that the parent body or bodies were either partially or fully differentiated, which is supported by the observation that the HSE patterns of the sHL and sHH subgroups are similar to some late-stage fractionates of the IIAB and IIIAB magmatic iron meteorite systems. Worsham et al. (2016a) suggested the sHL and sHH irons may have been produced by fractional crystallization in a manner similar to the processes that acted on magmatic iron systems. The difference in the abundances of Ni in these subgroups indicates that they formed from separate parental melts (Wasson and Kallemeyn, 2002). Therefore, irons from the sHL and sHH subgroups represent either metal which melted and coalesced into separate descending metal diapirs in the same or different parent bodies, or metal which formed cores on distinct parent bodies. The latter scenario is shown in Fig. 4. Fractional crystallization is plausible for either of these scenarios.

5.4. Mo isotopic compositions of IAB meteorites compared to other meteorites and implications for distinct nebular reservoirs

The various nebular isotopic reservoirs represented in the IAB complex and other meteorite groups may be characterized by their relative proportions of nucleosynthetic components using Mo isotopes. Generally, the Mo isotopic compositions in bulk meteorites appear to reflect variable *s*-process deficits, though *r*-process excesses have also been identified in type-B CAIs (Dauphas et al., 2002a; Burkhardt et al., 2011). The *r*-process excess in CAIs is characterized by depletion in ^{94}Mo, relative to the other Mo isotopes when they are normalized to ^{98}Mo/^{96}Mo. Moreover, it has recently been shown that the relative abundances of ^{94}Mo are variable at the bulk meteorite scale (Budde et al., 2016).

The CRE-corrected μ^{94}Mo and μ^{95}Mo of the IAB complex and our new data for grouped and ungrouped magmatic iron meteorites are shown in Fig. 5. The IAB data form a linear trend constituted by two clusters. The low Au IAB MG, subgroups, and winonaites plot near

μ^{94}Mo and μ^{95}Mo = 0 and are well resolved from magmatic iron groups. The high Au IAB subgroups form the second cluster around μ^{94}Mo of ~50–120 and μ^{95}Mo of ~20–50 ppm, along with IVA, IIIAB, and IC magmatic irons. Our new data for ordinary and enstatite chondrites and some primitive achondrites also plot within this cluster. Sombrerete plots in a third cluster with the IVB magmatic group, and ungrouped irons Chinga, Dronino, and Tishomingo at μ^{94}Mo values of ~150 and μ^{95}Mo values of ~100 ppm.

The trend defined by the IAB complex overlaps with a theoretical *s*-process deficit line, calculated here using the equations of Dauphas et al. (2004) and the stellar model of Arlandini et al. (1999). The agreement of these slopes is consistent with Dauphas et al. (2004) and Burkhardt et al. (2011), and it indicates that the trend reflects two-component mixing. The first component, characterized by an *s*-deficit, is potentially a homogenized nebular component (Dauphas et al., 2002b; Burkhardt et al., 2012). The second component may be “residue” left from thermal processing of the homogenized component, where volatile loss of thermally la-bile Mo oxides that were depleted in *s*-process Mo, or enriched in *r*- and *p*-process Mo, imparted a variably *s*-enriched isotopic signature, relative to the homogenized component (Burkhardt et al., 2012).

Sombrerete and the IVB and ungrouped meteorites do not fall on this line, consistent with the observations of Budde et al. (2016). These meteorites fall along a line defined by leachates of the carbonaceous chondrite Murchison (Burkhardt et al., 2012). Data for other carbonaceous chondrites also fall along this line, but type B CAIs, characterized by an *r*-process excess (Burkhardt et al., 2011), plot well above it (Fig. 5). Thus, the offset of these bulk iron meteorites and chondrites from the pure *s*-process deficit line indicates less depletion of ^{94}Mo, relative to ^{95}Mo than is observed in type B CAIs. This is consistent with mixing with a source which has both an *s*-process deficit and an enrichment of an *r*-process component (Budde et al., 2016).

The three distinct populations of meteorites may reflect a variety of presolar carriers representing both *s*- and *r*-process components and/or complex thermal processing which contributed to the isotopic signature recorded in the various meteorite groups. Variable thermal processing of mineralogically different presolar carriers may explain why the *s*-depleted (e.g., IAB) and the *s*-depleted/*r*-enriched (e.g., Sombrerete, IVB) components are distinct from one another. Alternately, the excess *r*-process component may be due to a late injection of *r*-process enriched materials from a nearby supernova (e.g., Dauphas et al., 2010; Budde et al., 2016). Because the *s*-depleted/*r*-enriched reservoirs are characterized by both volatile-rich carbonaceous chondrites and volatile-depleted IVB iron meteorites, late injection of *r*-process enriched material is more likely. Of note, most meteorites measured thus far, which have large Mo nucleosynthetic anomalies (μ^{97}Mo ≥ 40), plot on the line reflecting an excess *r*-component in addition to an *s*-deficit. Thus, large nucleosynthetic anomalies in Mo are generally associated with the *r*-process excess.

The Mo isotopic compositions of the MG, the sLL, sLM, and sLH subgroups, and the winonaites overlap with the terrestrial Mo isotopic composition. Palladium isotope data for some IAB MG and sLL irons also overlap with the terrestrial Pd isotopic composition (Mayer and Humayun, 2015), whereas μ^{100}Ru for the MG is narrowly resolved from the

Earth once CRE effects are taken into account (Fischer-Gödde and Kleine, 2017). Finally, $\Delta^{17}O$ in IAB silicates and winonaites are similar to, but well resolved from terrestrial (e.g., Clayton and Mayeda, 1996). Therefore, the isotopic genetic affinities between the IAB complex and Earth are limited to Mo, Pd, and possibly Ru, and do not apply to O isotopes. This may not be surprising given that O isotope variability is likely not nucleosynthetic in origin, whereas Mo, Pd, and Ru isotope variability is. Nevertheless, the close agreement of these isotope systems between the MG and low Au subgroups of the IAB complex with the isotopic composition of Earth makes these meteorites unique among iron meteorite groups and chondrites. Although enstatite chondrites have been promoted as representative precursor materials to Earth (e.g., Javoy, 1995), they have a resolvably higher $\mu^{97}Mo$ (Fig. 2), as well as resolved Ti isotopic compositions (Zhang et al., 2012). The H5 ordinary chondrites also have well resolved Mo isotopic compositions from Earth (Burkhardt et al., 2011; this work). Therefore, the present database suggests that much of the IAB complex represents Earth's closest genetic relation, due either to location in the nebula and/or the time at which precursor materials condensed.

6. Conclusions

The MG, sLL, sLM, and sLH subgroups have identical Mo isotopic compositions. The MG and sLL subgroup likely formed on the same parent body in separate metal segregation events. Highly siderophile element evidence suggests that the sLM and sLH subgroups formed on a separate parent body from the MG (Worsham et al., 2016a). Together, these data indicate that the nebular reservoir from which the MG and these subgroups formed was chemically heterogeneous, but isotopically homogeneous with respect to Mo. Tungsten-182 model ages indicate that the MG, and the sLL and sLM subgroups formed 3–5 Ma after CAI. These segregation ages are near the end of the effective lifetime of ^{26}Al, suggesting that the metallic melts by which the MG and sLL and sLM subgroups formed were generated by impact-induced melting.

The sHH and sHL subgroups have Mo isotopic compositions which overlap with each other, but are distinct from the MG. These meteorites also have model metal segregation ages between 0.3 and 1.6 Ma after CAI, that are within the effective lifetime of ^{26}Al. These meteorites likely formed in the fractionally crystallized cores, or large metal diapirs, of internally heated parent bodies.

Collectively, the pre-exposure Mo and W isotopic compositions, combined with HSE abundances (Worsham et al., 2016a), are consistent with the formation of IAB MG and subgroups on at least three separate parent bodies (Table S8). Moreover, at least three periods of metal-silicate segregation occurred to generate the various melts on the different parent bodies. While it is useful to think about the IAB complex in terms of similar processes, it can no longer be considered a genetically related family of meteorites. The IAB MG and the sLL, sLM, and sLH subgroups, along with winonaites constitute the only cosmochemical materials yet analyzed that share a Mo isotopic composition with the Earth, indicating that the parent bodies of these meteorites are the closest genetic relations to the precursor materials of the Earth.

Supplementary Material

Refer to Web version on PubMed Central for supplementary material.

Acknowledgements

We gratefully acknowledge the Smithsonian Institute National Museum of Natural History for providing the samples used in this study, and David Kring for providing NWA 725. Funding for this work was provided by NASA Cosmochemistry grant NNX13AF83G, NASA Emerging Worlds grant NNX16AN07G, and NASA SSERVI grant NNA14AB07A. We thank editor Bernard Marty and two anonymous reviewers for their helpful comments. We also thank Igor Puchtel, Richard Ash, and Mathieu Touboul for lab and analytical guidance; Kyle Ludwig and Jonathan Tino for sample preparation assistance; and Greg Archer for helpful discussions.

References

Allègre CJ, Luck J-M, 1980 Osmium isotopes as petrogenetic and geological tracers. Earth Planet. Sci. Lett 48, 148–154.

Archer GJ, Mundl A, Walker RJ, Worsham EA, Bermingham KR, 2017 High-precision analysis of $^{182}W/^{184}W$ and $^{183}W/^{184}W$ by negative thermal ionization mass spectrometry: per-integration oxide corrections using measured $^{18}O/^{16}O$. Int. J. Mass Spectrom 414, 80–86.

Arlandini C, Käppeler F, Wisshak K, Gallino R, Lugaro M, Busso M, Straniero O, 1999 Neutron capture in low-mass asymptotic giant branch stars: cross sections and abundance signatures. Astrophys. J 525, 886–900.

Benedix GK, McCoy TJ, Keil K, Love SG, 2000 A petrologic study of the IAB iron meteorites: constraints on the formation of the IAB-winonaite parent body. Meteorit. Planet. Sci 35, 1127–1141.

Bild RW, 1977 Silicate inclusions in group IAB irons and a relation to the anomalous stones Winona and Mt Morris (Wis). Geochim. Cosmochim. Acta 41, 1439–1456.

Birck J-L, Roy-Barman M, Capmas F, 1997 Re–Os isotopic measurements at the femtomole level in natural samples. Geostand. Newsl 20, 9–27.

Budde G, Burkhardt C, Brennecka GA, Fischer-Gödde M, Kruijer TS, Kleine T, 2016 Molybdenum isotopic evidence for the origin of chondrules and a distinct genetic heritage of carbonaceous and non-carbonaceous meteorites. Earth Planet. Sci. Lett 454, 293–303.

Burbidge EM, Burbidge GR, Fowler WA, Hoyle F, 1957 Synthesis of the elements in stars. Rev. Mod. Phys 29, 547–650.

Burkhardt C, Kleine T, Oberli F, Pack A, Bourdon B, Wieler R, 2011 Molybdenum isotope anomalies in meteorites: constraints on solar nebula evolution and origin of the Earth. Earth Planet. Sci. Lett 312, 390–400.

Burkhardt C, Kleine T, Dauphas N, Wieler R, 2012 Origin of isotopic heterogeneity in the solar nebula by thermal processing and mixing of nebular dust. Earth Planet. Sci. Lett 357, 298–307.

Clayton RN, Mayeda TK, 1996 Oxygen isotope studies of achondrites. Geochim. Cosmochim. Acta 60, 1999–2017.

Cohen AS, Waters FJ, 1996 Separation of osmium from geological materials by solvent extraction for analysis by thermal ionization mass spectrometry. Anal. Chim. Acta 332, 269–275.

Cook DL, Walker RJ, Horan MF, Wasson JT, Morgan JW, 2004 Pt–Re–Os systematics of group IIAB and IIIAB iron meteorites. Geochim. Cosmochim. Acta 68, 1413–1431.

Dauphas N, Marty B, Reisberg L, 2002a Molybdenum evidence for inherited planetary scale isotope heterogeneity of the protosolar nebula. Astrophys. J 565, 640–644.

Dauphas N, Marty B, Reisberg L, 2002b Molybdenum nucleosynthetic dichotomy revealed in primitive meteorites. Astrophys. J 569, L139–L142.

Dauphas N, Davis AM, Marty B, Reisberg L, 2004 The cosmic molybdenum–ruthenium isotope correlation. Earth Planet. Sci. Lett 226, 465–475.

Dauphas N, Remusat L, Chen JH, Roskosz M, Papanastassiou D, Stodolna J, Guan Y, Ma C, Eiler JM, 2010 Neutron-rich chromium isotope anomalies in supernova nanoparticles. Astrophys. J 720, 1577–1591.

Fischer-Gödde M, Burkhardt C, Kruijer TS, Kleine T, 2015 Ru isotope heterogeneity in the solar protoplanetary disk. Geochim. Cosmochim. Acta 168, 151–171.

Fischer-Gödde M, Kleine T, 2017 Ruthenium isotopic evidence for an inner solar system origin of the late veneer. Nature 541, 525–527. [PubMed: 28128236]

Greenwood RC, Franchi IA, Gibson JM, Benedix GK, 2012 Oxygen isotope variation in primitive achondrites: the influence of primordial, asteroidal and terrestrial processes. Geochim. Cosmochim. Acta 94, 146–163.

Javoy M, 1995 The integral enstatite chondrite model of the Earth. Geophys. Res. Lett 22, 2219–2222.

Kleine T, Mezger K, Münker C, Palme H, Bischoff A, 2004 ^{182}Hf–^{182}W isotope systematics of chondrites, eucrites, and Martian meteorites: chronology of core formation and mantle differentiation in Vesta and Mars. Geochim. Cosmochim. Acta 68, 2935–2946.

Kruijer TS, Touboul M, Fischer-Gödde M, Bermingham KR, Walker RJ, Kleine T, 2014a Protracted core formation and rapid accretion of protoplanets. Science 344, 1150–1154. [PubMed: 24904163]

Kruijer TS, Kleine T, Fischer-Gödde M, Burkhardt C, Wieler R, 2014b Nucleosynthetic W isotope anomalies and the Hf–W chronometry of Ca–Al-rich inclusions. Earth Planet. Sci. Lett 403, 317–327.

Lee D-C, Halliday AN, 1996 Hf–W isotopic evidence for rapid accretion and differentiation in the early solar system. Science 274, 1876–1879. [PubMed: 8943194]

Lee T, Papanastassiou DA, Wasserburg GJ, 1977 Aluminum-26 in the early solar system: fossil or fuel? Astrophys. J 211, L107–L110.

Lovering JF, 1957 Differentiation in the iron–nickel core of a parent meteorite body. Geochim. Cosmochim. Acta 12, 238–252.

Lu Q, Masuda A, 1994 The isotopic composition and atomic weight of molybdenum. Int. J. Mass Spectrom. Ion Process 130, 65–72.

Ludwig KR, 2003 User's Manual for Isoplot 3.00. Berkeley Geochronology Center Special Publication No. 4, Berkeley, CA, 70 pp.

Markowski A, Quitté G, Halliday AN, Kleine T, 2006 Tungsten isotopic compositions of iron meteorites: chronological constraints vs. cosmogenic effects. Earth Planet. Sci. Lett 242, 1–15.

Masarik J, 1997 Contribution of neutron-capture reactions to observed tungsten isotopic ratios. Earth Planet. Sci. Lett 152, 181–185.

Mayer B, Humayun M, 2015 Nucleosynthetic anomalies in palladium from IAB, IVA, and IVB iron meteorites. Lunar Planet. Sci. Conf. Abstr 46, 1265.

McCoy TJ, Keil K, Scott ERD, Haack H, 1993 Genesis of the IIICD iron meteorites: evidence from silicate-bearing inclusions. Meteoritics 28, 552–560.

Norris TL, Gancarz AJ, Rokop DJ, Thomas KW, 1983 Half-life of ^{26}Al. Proc. Lunar Planet. Sci. Conf 14, B331–B333.

Qin L, Dauphas N, Horan MF, Leya I, Carlson RW, 2015 Correlated cosmogenic W and Os isotopic variations in Carbo and implications for Hf–W chronology. Geochim. Cosmochim. Acta 153, 91–104.

Ruzicka A, Hutson M, Floss C, 2006 Petrology of silicate inclusions in the Sombrerete ungrouped iron meteorite: implications for the origins of IIE-type silicate-bearing irons. Meteorit. Planet. Sci 41, 1797–1831.

Schulz T, Upadhyay D, Münker C, Mezger K, 2012 Formation and exposure history of non-magmatic iron meteorites and winonaites: clues from Sm and W isotopes. Geochim. Cosmochim. Acta 85, 200–212.

Scott ERD, 1972 Chemical fractionation in iron-meteorites and its interpretation. Geochim. Cosmochim. Acta 36, 1205–1236.

Touboul M, Walker RJ, 2012 High precision tungsten isotope measurement by thermal ionization mass spectrometry. Int. J. Mass Spectrom 309, 109–117.

Trinquier A, Elliott T, Ulfbeck D, Coath C, Krot AN, Bizzarro M, 2009 Origin of nucleosynthetic isotope heterogeneity in the solar protoplanetary disk. Science 324, 374–376. [PubMed: 19372428]

Vockenhuber C, Oberli F, Bichler M, Ahmad I, Quitté G, Meier M, Halliday AN, Lee DC, Kutschera W, Steier P, Gehrke RJ, Helmer RG, 2004 New half-life measurement of ^{182}Hf: improved chronometer for the early solar system. Phys. Rev. Lett 93, 172501. [PubMed: 15525068]

Volkening J, Köppe M, Heumann KG, 1991 Tungsten isotope ratio determinations by negative thermal ionization mass spectrometry. Int. J. Mass Spectrom 107, 361–368.

Walker RJ, 2012 Evidence for homogeneous distribution of osmium in the proto-solar nebula. Earth Planet. Sci. Lett 351, 36–44.

Wasson JT, Kallemeyn GW, 2002 The IAB iron-meteorite complex: a group, five subgroups, numerous grouplets, closely related, mainly formed by crystal segregation in rapidly cooling melts. Geochim. Cosmochim. Acta 66, 2445–2473.

Wittig N, Humayun M, Brandon AD, Huang S, Leya I, 2013 Coupled W–Os–Pt isotope systematics in IVB iron meteorites: in situ neutron dosimetry for W isotope chronology. Earth Planet. Sci. Lett 361, 152–161.

Worsham EA, Bermingham KR, Walker RJ, 2016a Siderophile element systematics of IAB complex iron meteorites: new insights into the formation of an enigmatic group. Geochim. Cosmochim. Acta 188, 261–283.

Worsham EA, Walker RJ, Bermingham KR, 2016b High-precision molybdenum isotope analysis by negative thermal ionization mass spectrometry. Int. J. Mass Spectrom 407, 51–61.

Yin Q, Jacobsen SB, Yamashita K, 2002 Diverse supernova sources of pre-solar material inferred from molybdenum isotopes in meteorites. Nature 415, 881–883. [PubMed: 11859361]

Zhang J, Dauphas N, Davis AM, Leya I, Fedkin A, 2012 The proto-Earth as a significant source of lunar material. Nat. Geosci 5, 251–255.

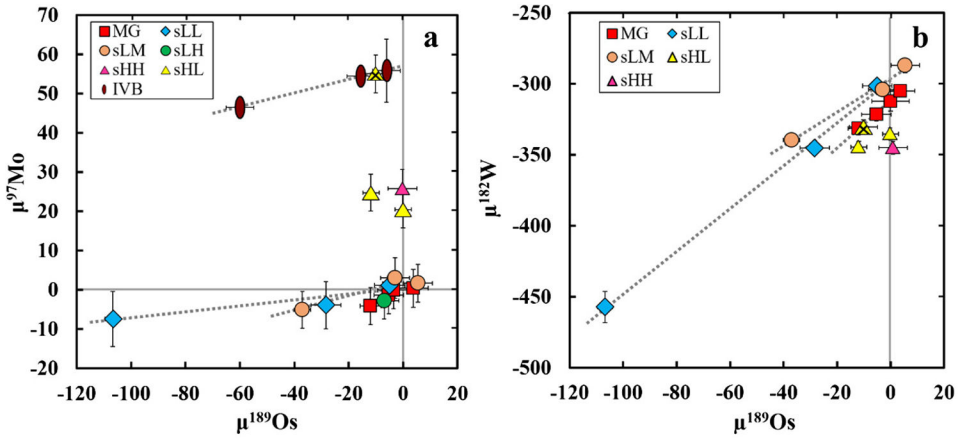

Fig. 1.

(a) μ^{189}Os vs. μ^{97}Mo, and (b) μ^{189}Os vs. μ^{182}W used for CRE correction, using data from Tables 1, S2–S4. Duplicate analyses are averaged and used in the linear regressions. In (a) the linear regressions are shown for the sLL and sLM subgroups and the IVB magmatic iron meteorite group, using data from this work. In (b) regressions are shown for the MG and the sLL and sLM subgroups. Sombrerete is denoted with the crossed yellow triangle symbol. Slopes and intercepts of each regression are given in Tables S5–S6. Uncertainties of the standards are not shown for clarity, but are ~6 ppm for μ^{189}Os and ~5 ppm for μ^{97}Mo and μ^{182}W. Error bars are the 2SD of the standards or the 2SD or 2SE of multiple analyses. (For interpretation of the references to color in this figure legend, the reader is referred to the web version of this article.)

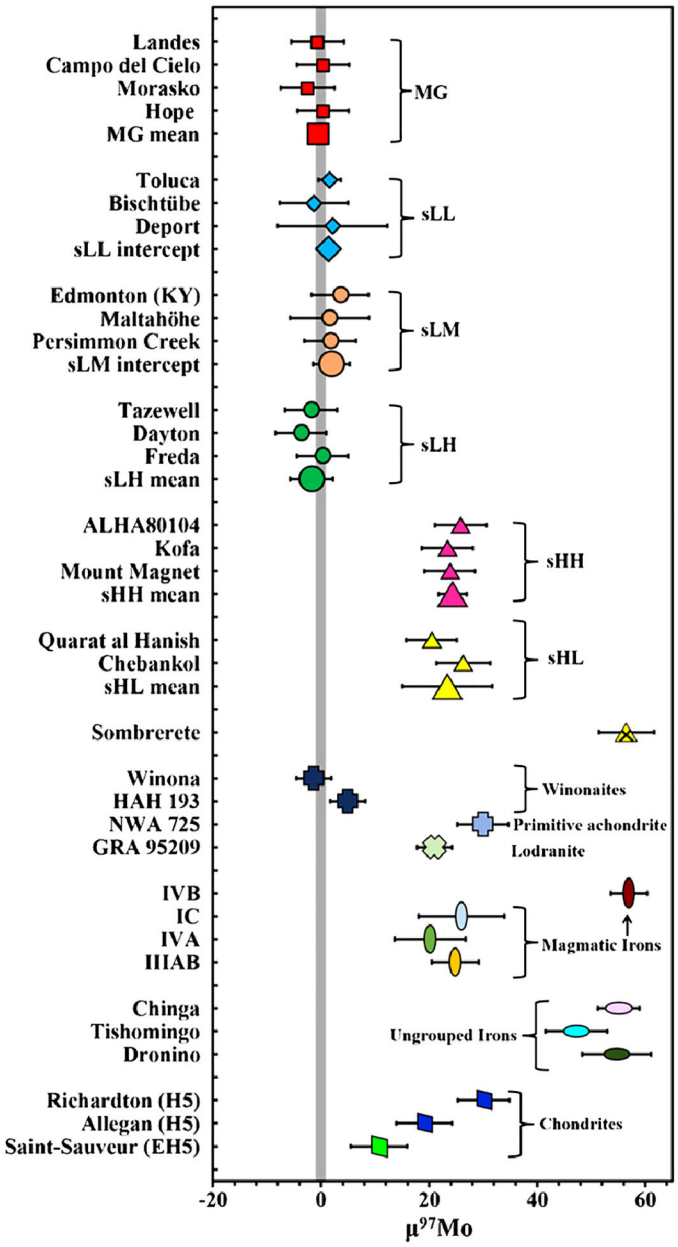

Fig. 2.

Pre-exposure μ^{97}Mo for the IAB complex iron meteorites. Shown for comparison are the μ^{97}Mo values of primitive achondrites, magmatic iron meteorite groups, ungrouped iron meteorites, and chondrites from this study. The light grey bar is the 2SE of repeated analyses of terrestrial standards. Error bars for each sample here and in Fig. 3 are the propagated 2SD or 2SE uncertainties (see text and Table 2 for details).

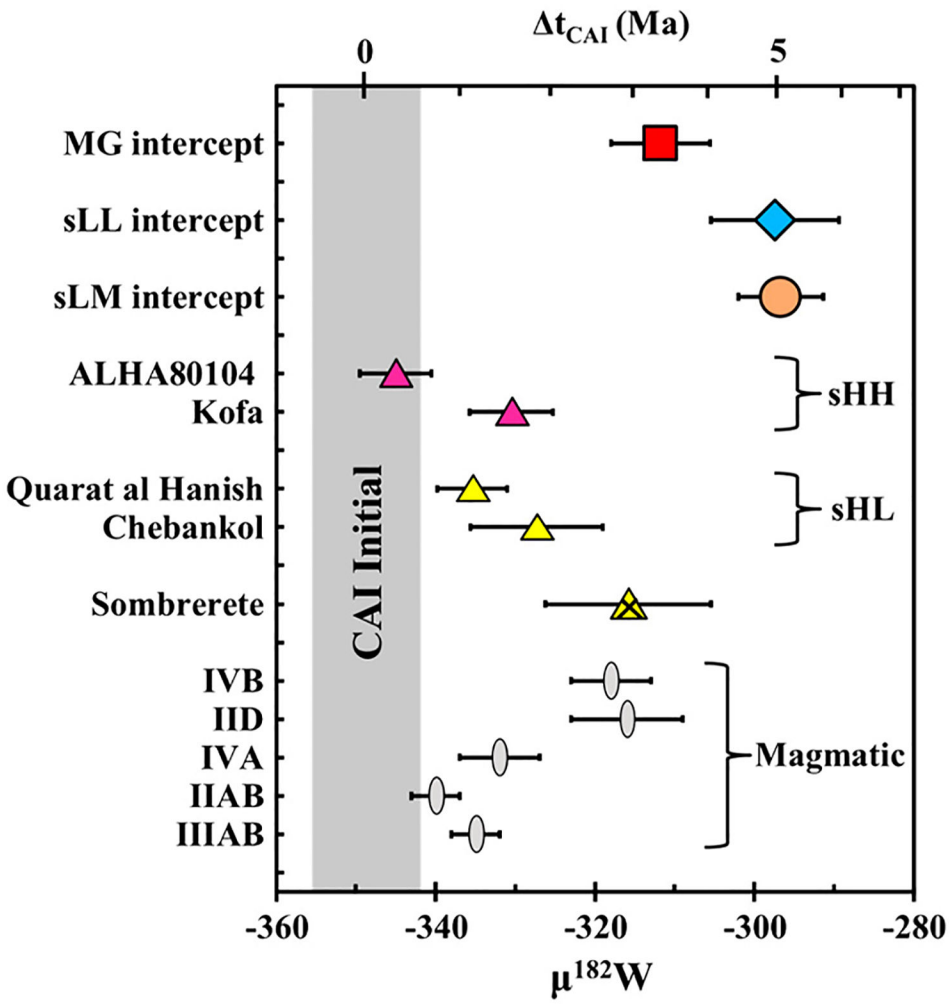

Fig. 3.

Cosmic ray exposure-corrected μ^{182}W for IAB complex meteorites. For the MG and sLL and sLM subgroups, the intercept-derived, group pre-exposure μ^{182}W, as determined using the linear regression of μ^{189}Os vs. μ^{182}W, are shown. Other meteorites were corrected using a slope averaged from MG, sLL, and sLM trends. Magmatic iron meteorite groups are shown for comparison (from Kruijer et al., 2014a). The CAI initial μ^{182}W value is from Kruijer et al. (2014b).

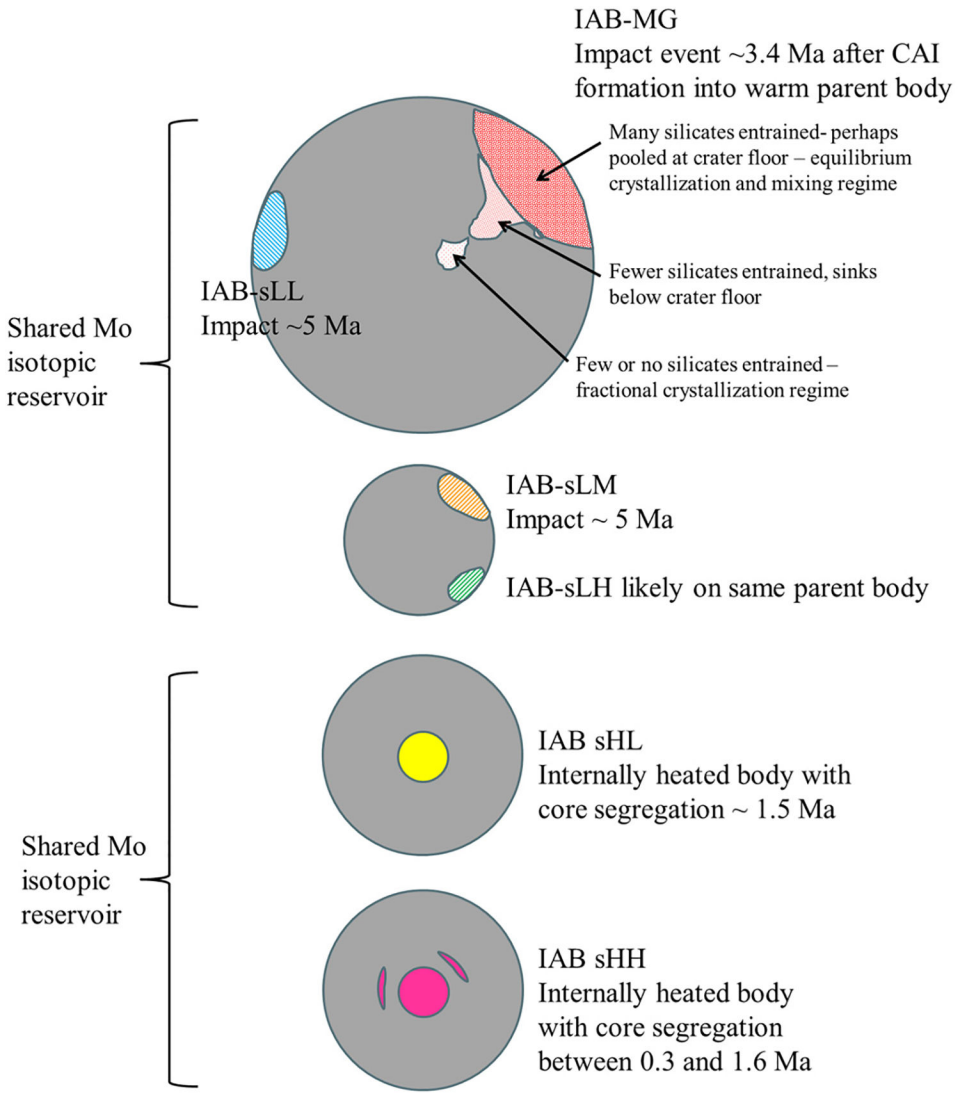

Fig. 4.

Idealized IAB complex parent bodies with the preferred formation mechanisms for the MG and each of the subgroups, combining evidence from Mo and W isotope data (this study) with HSE data and observed silicate distributions among MG irons (Worsham et al., 2016a). Winonaites likely formed on the MG-sLL parent body (McCoy et al., 1993; Benedix et al., 2000). Relative parent body sizes are arbitrary.

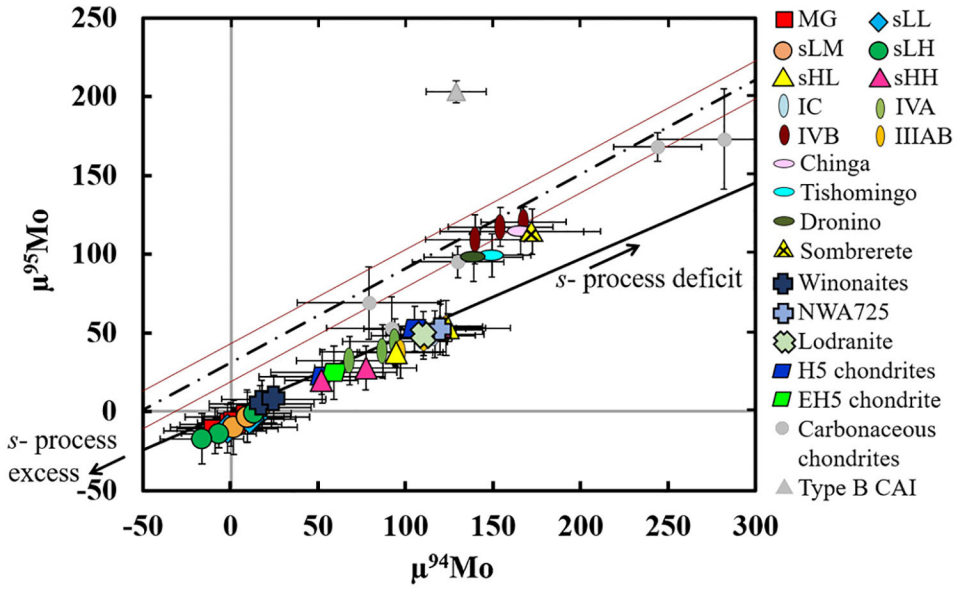

Fig. 5.

CRE corrected μ^{94}Mo vs. μ^{95}Mo for IAB complex meteorites, primitive achondrites, magmatic iron meteorite groups, and chondrites. Carbonaceous chondrite and type B CAI data are from Burkhardt et al. (2011). The solid black line is a theoretical mixing line between a pure *s*-process deficit component and an *s*-process excess component calculated using equations from Dauphas et al. (2004) and data from Arlandini et al. (1999). The dashed line is the linear regression through Murchison leachate data (Burkhardt et al., 2012), plotted with the error envelope (red lines). Three different nebular reservoirs are evident. Variations in the Mo isotope ratios are due to both variable depletions in the *s*-process component, and deviations in the relative abundances of the *r*-process and *s*-process components. (For interpretation of the references to color in this figure legend, the reader is referred to the web version of this article.)

Table 1

μ^{189}Os and μ^{190}Os data for IAB complex meteorites. Osmium isotope data for other iron meteorites are reported in Table S2.

Sample	n^a	μ^{189}Os	2SD	μ^{190}Os	2SD
MG					
Canyon Diablo[a]	1	0	7	3	5
Landes	2	−5	5	2	6
Campo del Cielo	2	4	5	1	6
Bogou	2	−7	5	−1	9
Morasko	3	−12	4	3	3
Hope	1	−4	6	7	4
sLL					
Toluca	4	−5	6	1	3
Bischtube	3	−28	5	16	8
Deport	3	−107	3	59	4
sLM					
Edmonton (KY)	1	−3	5	0	3
Maltahöhe	1	−37	3	18	5
Persimmon Creek	2	5	5	−9	3
sLH					
Tazewell	1	−7	5	−10	3
sHH					
ALHA 80104	1	0	5	−5	3
sHL					
Quarat al Hanish	1	0	3	−1	5
Chebankol	1	−12	3	−5	5
Sombrerete	1	−10	5	2	3

[a] *n* is the number of analyses. Data for Canyon Diablo are from Walker (2012). Uncertainties for samples analyzed once are 2SD of the standards run in the same analytical campaign. For 2–3 analyses, the uncertainties are either the 2SD of the standards or of the analyses, whichever is larger. Uncertainties for samples measured >3 times are the 2SE.

Table 2

The CRE-corrected Mo isotopic compositions of IAB complex iron meteorites and other meteorites.

Sample	n^a	μ^{92}Mo	±	μ^{94}Mo	±	μ^{95}Mo	±	μ^{97}Mo	±	μ^{100}Mo	±
MG											
Landes	1	−35	2	−9	29	−12	14	−0.7	4.9	1	34
Campo del Cielo[b]	1	−28	2	0	29	−8	14	0.4	4.8	−4	34
Morasko	1	−8	71	2	21	−7	9	−2.5	5.0	−5	31
Hope	1	12	68	10	25	−3	17	0.4	4.8	11	30
MG mean		−15	21	1	8	−8	4	−0.6	1.4	1	7
sLL											
Toluca	3	15	45	13	17	−4	6	1.5	2.1	1	3
Bischtube	1	−33	2	−2	29	−11	15	−1.4	6.3	−3	24
Deport	2	10	83	11	27	−5	7	2	10	−2	28
sLL intercept		7	44	10	16	−5	6	1.3	2.1	−1	5
sLM											
Edmonton (KY)	2	−27	110	2	36	−10	17	3.5	5.3	−3	33
Maltahöhe	1	0	117	10	35	−3	16	1.5	7.3	−1	31
Persimmon Creek[b]	1	18	92	17	29	2	14	1.7	4.8	1	34
sLM intercept		−3	66	9	21	−4	10	1.9	3.4	−1	4
sLH											
Tazewell	1	−55	71	−7	21	−14	9	−1.8	4.8	−8	31
Dayton[c]	1	1	71	14	21	−1	9	−3.7	4.7	−1	31
Freda[c]	1	−58	68	−16	24	−17	16	0.3	4.7	−9	30
sLH mean		−31	88	−3	31	−11	17	−1.8	4.0	−6	9
sHH											
ALHA 80104[b]	2	44	92	77	29	28	14	26	5	5	34
Kofa[c]	1	8	71	52	21	20	9	23	5	3	31
Mount Magnet[c]	1	173	68	120	24	54	16	24	5	42	30
sHH mean		75	173	83	69	34	36	24	3	16	44

Earth Planet Sci Lett. Author manuscript; available in PMC 2019 January 30.

Sample	n^a	μ^{92}Mo	±	μ^{94}Mo	±	μ^{95}Mo	±	μ^{97}Mo	±	μ^{100}Mo	±
sHL											
Quarat al Hanish[b]	1	88	71	95	21	37	9	20	5	30	31
Chebankol	1	166	71	124	21	53	9	26	5	40	31
sHL mean		127	111	109	42	45	22	23	8	35	14
Sombrerete	1	220	93	173	29	115	15	57	5	72	34
Primitive achondrites											
Winona (Win)[c]	1	20	90	18	30	5	15	−1.3	3.3	1	22
HAH 193 (Win)[c]	1	40	90	25	30	8	15	4.9	3.3	5	22
NWA 725[c]	1	155	68	120	24	52	16	30	5	63	30
GRA 95209 (Lod)[c]	1	148	90	110	30	48	15	21	3	24	22
Magmatic groups											
IVB intercept	9 (3)	247	76	155	22	117	10	57	3	84	33
IC	2 (1)	172	91	117	29	49	16	26	8	37	24
IVA	3 (3)	104	73	83	27	38	12	20	7	24	30
IIIAB	5 (3)	141	72	110	26	46	16	25	4	44	24
Ungrouped iron meteorites											
Chinga	2	231	148	166	46	114	15	55	4	77	56
Tishomingo	2	216	94	149	22	99	14	47	6	75	49
Dronino	1	162	90	139	28	98	15	55	6	63	24
Chondrites											
Richardton metal (H5)[c]	1	100	92	105	29	53	14	30	5	11	34
Allegan (H5)[c]	1	43	110	52	36	22	17	19	5	21	33
Saint-Sauveur (EH5)[c]	1	103	110	59	36	25	17	11	5	42	33

[a] n is the number of analyses. For the magmatic iron meteorite groups, the number of analyses is given first, followed in parentheses by the number of iron meteorites representing the group. The uncertainties are the 2SD ($n \leq 3$) or 2SE ($n > 3$). The uncertainties shown here for individual meteorites were propagated through the CRE correction calculation, accounting for the uncertainties of the measurements and the slopes. Due to the lack of a correlation between ^{189}Os and ^{100}Mo, ^{100}Mo is not corrected for CRE.

[b] Samples for which μ^{189}Os was $\succ -1$ were not CRE-corrected (see SM section 3 for details).

[c] Os isotope data were not obtained for these samples, so they are not corrected for CRE (see SM section 3 for details).

Earth Planet Sci Lett. Author manuscript; available in PMC 2019 January 30.

Table 3

Cosmic ray exposure-corrected μ^{182}W isotopic compositions and model ages for IAB complex iron meteorites.

Sample	Method[a]	*n*	$\mu^{182}W_{186/183}$	±	$\mu^{182}W_{186/184}$	±	Δt_{CAI}	±
MG								
Canyon Diablo[b]	I	1	−312	7	−311	9	3.4	0.7
Landes	I	1	−313	11	−314	10	3.3	1.1
Campo del Cielo[b]	I	1	−305	5	−305	6	4.1	0.5
Morasko	II	1	−311	12	−318	10	3.5	1.3
MG intercept			−312	6			3.4	0.7
sLL								
Toluca	I	2	−294	10	−293	10	5.4	1.2
Bischtübe	II	1	−302	10	−311	11	4.5	1.2
Deport	I, II	2	−295	16	−298	17	5.3	2.0
Goose Lake[c]	I	1	−298	6	−303	8	4.9	0.8
sLL intercept			−297	8			5.0	1.0
sLM								
Edmonton (KY)	II	1	−301	7	−305	9	4.6	0.9
Maltahöhe	II	1	−296	9	−298	10	5.2	1.1
Persimmon Creek[b]	I	1	−287	5	−288	6	6.3	0.7
sLM intercept			−297	5			5.1	0.6
sHH								
ALHA80104[b]	I	1	−345	5	−345	6	0.3	0.4
Kofa[c]	II	1	−330	5	−335	7	1.6	0.5
sHL								
Quarat al Hanish[b]	II	1	−335	4	−331	7	1.1	0.4
Chebankol	II	1	−327	8	−327	9	1.9	0.8
Sombrerete	I	2	−316	10	−315	11	3.0	1.1

[a]Method I used a second-order correction to account for variable oxygen isotope compositions between analyses. Method II measured the oxygen isotopic composition *in situ* as described in text. Uncertainties are as in Tables 1 and 2.

[b] Samples for which μ^{189}Os was >1 were not CRE-corrected (see SM section 3 for details).

[c] Samples for which Os isotope data were not obtained, and are, thus, not corrected for CRE (see SM section 3 for details). Goose Lake was not included in the calculation of the sLL intercept.